Turbulent Moisture Measurements aboard Instrumented Aircraft with a Capacitive Sensor

PIERRE DURAND

Laboratoire d'Aérologie, (URA CNRS 354) Université Paul Sabatier, Toulouse, France

GABRIEL ABADIE

CNRM, Météo-France, Toulouse, France

AIMÉ DRUILHET

Laboratoire d'Aérologie, (URA CNRS 354) Université Paul Sabatier, Toulouse, France

9 June 1994 and 8 December 1994

ABSTRACT

The authors show how a capacitive device measuring moisture can be used aboard instrumented atmospheric aircraft as an alternate sensor for turbulence measurement. Using a calibrated Lyman-α sensor as a reference, the time response of the capacitive device can be improved in such a way that turbulent latent heat flux and moisture variance can be calculated with a good level of accuracy. This improvement is done by correction of the amplitude as well of the phase of the signal. These corrections are determined from in-flight measurements; therefore, they take into account the time response of the sensor itself, as well as its airborne installation.

1. Introduction

Accurate measurements of latent heat flux in the atmospheric boundary layer (ABL) is of considerable interest from a climatic point of view. Many areas of investigation, such as air–sea exchange, or mesoscale hydrological budget, necessitate in situ measurement of latent heat flux on such a geographic scale that aircraft, at present, represent the only available instrument to achieve this goal. For more than 20 years, the eddy correlation technique has been successfully used on instrumented aircraft in order to determine turbulent fluxes (Lenschow 1970; Nicholls 1978; Druilhet et al. 1983): latent heat flux is calculated from the measurement of fluctuations in vertical air velocity and moisture. The latter is generally measured by a so-called "Lyman-α" device, which is calibrated against a dewpoint hygrometer (Buck 1976; Friehe et al. 1986; Weinheimer and Schwiesow 1992).

Calculation of turbulent flux by the eddy correlation method requires the measurement of turbulent fluctuations throughout the wavelength band contributing to the transfer: this wavelength band depends on the altitude above the ground, the stability of the ABL, etc. In other words, the fluctuations have to be measured in the band where the cospectrum of both variables is significant. To give an order of magnitude, in the ABL, this wavelength band extends from some 10 m to several kilometers (this is only an order of magnitude and cannot be considered as a rule!). So, given the airspeed of the instrumented aircraft (typically 100 m s^{-1}), we see that we must use sensors with a good time response between 0.1 and 100 s. The Lyman-α sensor satisfies this constraint, and it is widely used aboard atmospheric research aircraft. However, it has two main drawbacks: it requires flight-by-flight absolute calibration (Lind and Shaw 1991) and it can be unreliable. The first difficulty can be solved by routine calibration against a dewpoint hygrometer: although this sensor has a slow time response (some seconds in the ABL), it is an absolute reference. The second one is more problematic: namely, that the sensor could fail during flight.

During a major cooperative experiment, in November 1990 (see later), the Lyman-α device, installed aboard a French instrumented aircraft, failed during two flights. Considering the major importance of these flights, and particularly that of the latent heat flux computation, a technique was developed for deriving this parameter from another sensor (capacitive device). The calibration, described in this paper, was performed with the data from a preceeding flight, during which the two sensors operated simultaneously, and which was performed in similar conditions. This calibration was then successfully applied to the two flights with a failing Lyman-α.

Corresponding author address: Dr. Pierre Durand, Laboratoire d'Aérologie, Université Paul Sabatier, 118 Route de Narbonne, F31062 Toulouse, Cedex, France.
E-mail: durp@aero.ups-tlse.fr

2. Instrumentation and data

The aircraft used in this study is the Merlin IV of Météo-France (C.A.M. 1989; André and LePipec 1989). It is equipped with a radome on the nose, allowing the measurement of dynamic pressure, static pressure, and angles of attack and sideslip, following the principle described by Brown et al. (1983). An inertial navigation system (SAGEM ULIS 45i) measures the ground speeds and attitude angles of the aircraft. The mean and turbulent air velocities are then calculated following the classical method (Lenschow 1970). The air temperature is measured by a Rosemount 102E2AL probe and corrected for the adiabatic heating due to airspeed. After anti-aliaising analog filtering, signals used for turbulence computation were digitized and recorded at a sampling rate of 25 s^{-1}.

For moisture measurement, in this study, we used three sensors:

1) a dewpoint (T_d) hygrometer (General Eastern), used as the "slow" reference;

2) a Lyman-α "AIR" hygrometer, measuring the water vapor density fluctuation;

3) a capacitive sensor, measuring the relative humidity H.

The last of these three instruments was designed by the French Meteorological Office. Its characteristics and the necessary corrections are described in Abadie (1984) and in Abadie et al. (1991). Hence, our description is brief: it consists of a polymer sheet whose capacitance (typically 460 pF ±10%) varies with moisture. An oscillator translates the capacitance variations, so that the output frequency is a linear function of the relative humidity. The device is installed in a Rosemount 102-E housing. The following corrections are necessary to calculate the "true" ambient moisture from the raw signal.

1) A temperature correction, taking into account the sensitivity of the sensor to the temperature. This correction is linear and is calibrated in the laboratory:

$$H_t = H_i + a(20 - T_t), \tag{1}$$

where H_i is the indicated humidity, and H_t and T_t the humidity and temperature (°C) around the sensor. Here a is a constant of about 0.2.

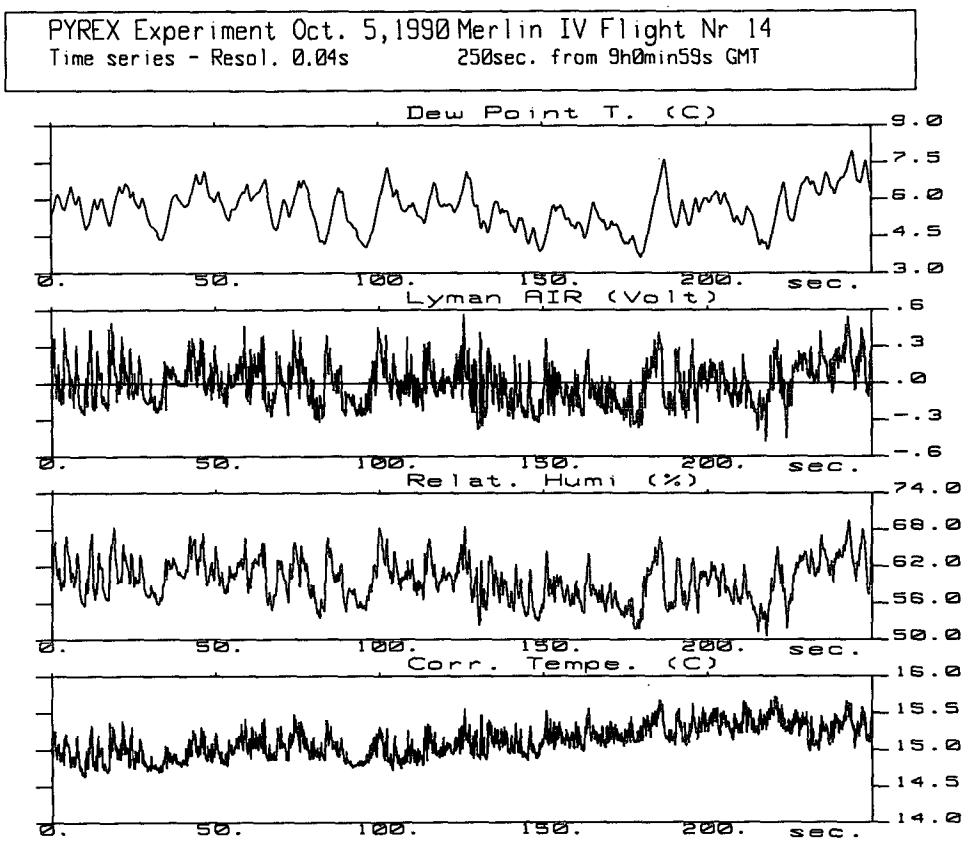

FIG. 1. Time series of a 250-s sample performed at about 40 m above the sea surface. The time resolution is 0.04 s. From top to bottom: dewpoint temperature (°C); raw signal (V) of the Lyman-α; relative humidity (%), corrected according to Eq. (3); and static air temperature (°C), corrected for heating due to airspeed.

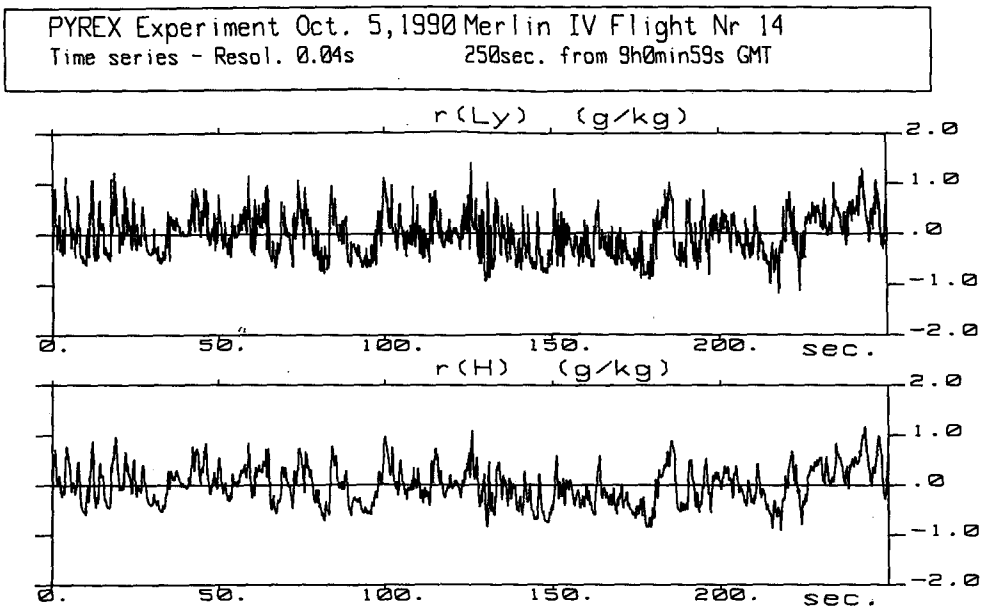

FIG. 2. On the same sample as Fig. 1, humidity mixing ratio (g kg^{-1}) calculated from the Lyman-α calibrated against the dewpoint hygrometer (top), and calculated from the capacitive sensor (bottom).

2) A dynamic correction: we suppose that the velocity of the flow with respect to the probe is low—that is, the pressure is close to the total pressure P_t, and the temperature close to the total temperature T_t (in other words, we suppose that the recovery factor of the housing is close to one, which seems reasonable considering the Rosemount housing). The humidity mixing ratio r can then be expressed as follows:

$$r = 0.622 \frac{He(T)}{P_s - He(T)} = 0.622 \frac{H_t e(T_t)}{P_t - H_t e(T_t)}, \quad (2)$$

where T and P_s are the static temperature and static pressure of the flow, respectively, H is the "true" humidity of the flow (at the temperature T and pressure P_s), and e is the vapor pressure. The assumption that the recovery factor is close to one requires justification. In fact, this term is of importance as regards the mean value of the mixing ratio, but has little consequence on its fluctuations, which are used in the latent heat flux computation.

Combining (1) and (2), we can express the true humidity H of the flow as a function of the indicated humidity H_i:

$$H = [H_i + a(20 - T_t)] \frac{e(T_t)}{e(T)} \frac{P_s}{P_t}. \quad (3)$$

From the dewpoint temperature, we calculate r:

$$r = 0.622 \frac{e(T_d)}{P - e(T_d)}, \quad (4)$$

where P is the air pressure around the sensor (generally the total pressure P_t). The Lyman-α signal is then calibrated against this function (4), by a simple linear regression, after averaging both signals at a resolution of several seconds, so that they have compatible bandpass. (This calibration does not include density fluctuations, whose repercussions on mixing ratio fluctuations are negligible in this case.) The result is called r_{Ly}. The humidity mixing ratio can also be calculated from the humidity H using (2): we will call it r_H.

The data were gathered during the PYREX experiment (Bougeault et al. 1993). The main goal of this experiment was to study the effect of a mountain range (the Pyrenees) on the atmospheric flow at mesoscale. One of the objectives was to study the dynamics of local winds caused by the effect of relief on the flow. One of these winds (the tramontana) was examined over the Mediterranean Sea. The data used for the calibration of the capacitive device relate to 5 October 1990 (flight 14). The general situation was a north synoptic flow, with the tramontana wind blowing over the Mediterranean Sea at about 20 m s^{-1} in the ABL. Over the flight area, the mean sensible heat flux at the sea surface was about 50 W m^{-2}, the mean latent heat flux 450 W m^{-2}, and the friction velocity 0.78 m s^{-1}. The turbulence energy in the ABL was very high, both for velocities and moisture.

3. Turbulent moisture

Figure 1 presents the thermodynamic data used for turbulence calculations on a sample of 250 s (about 24 km): corrected static temperature (including adiabatic correction due to the airspeed of the aircraft), corrected relative humidity measured by the capacitive

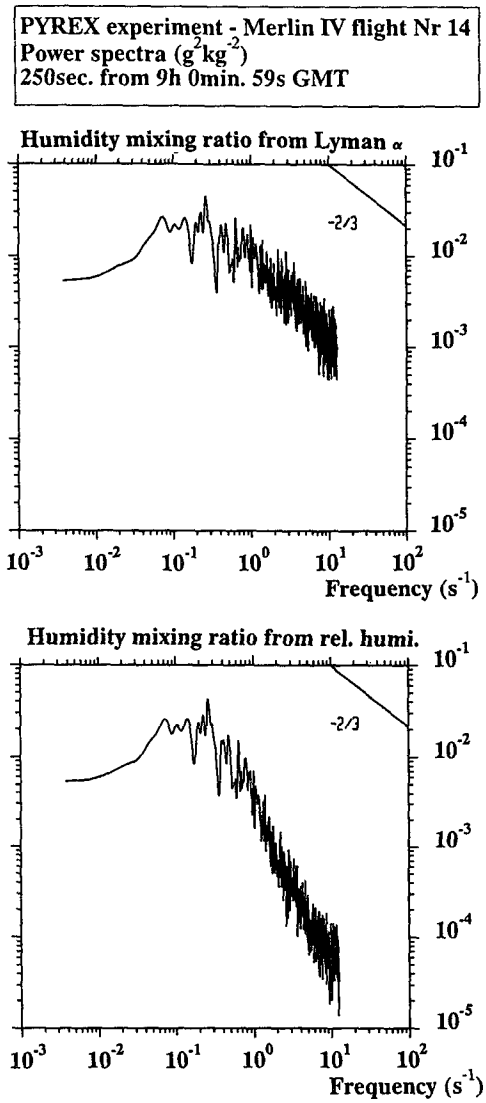

FIG. 3. Power spectra of the humidity mixing ratio [$nS(n)$, (g^2 kg^{-2})] calculated from the Lyman-α calibrated against the dewpoint hygrometer (top), and calculated from the capacitive sensor (bottom), as a function of the frequency (s^{-1}). The straight line is the $-2/3$ power law. Same sample as Fig. 1.

sensor (including the corrections mentioned above), the raw signal from the Lyman-α (without calibration), and the dewpoint temperature. These four signals are used in the study. Note the lag of the dewpoint temperature with respect to the Lyman-α (about 2 s) and the difference in time response between the two sensors. Fluctuations in the humidity mixing ratio, as calculated by the two techniques mentioned above, are shown in Fig. 2. The linear trend was removed. Although both signals present a very high correlation, we see that the Lyman-α signal (hereafter r_{Ly}) has higher spectral levels than the other one (hereafter r_H), which is confirmed by the energy spectra (Fig. 3): r_{Ly} follows the $-2/3$ power law, characteristic of the inertial subrange, up

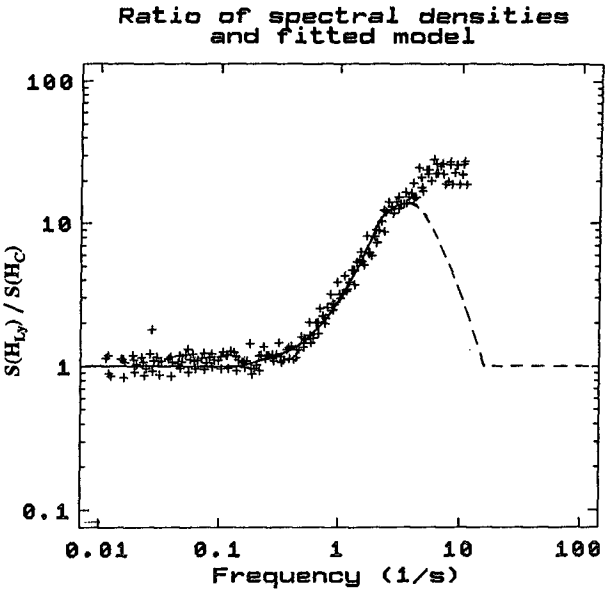

FIG. 4. Spectral energy ratio of the relative humidity calculated from the calibrated Lyman-α to that calculated from the capacitive sensor, as a function of the frequency (s^{-1}). The solid and dashed line are the correction applied to the capacitive signal. Log–log coordinates.

to the upper limit of frequency, whereas for r_H there is significant attenuation from about 0.3 s^{-1}, preventing accurate calculation of the latent heat flux. However, the signal can be present, although attenuated, at higher

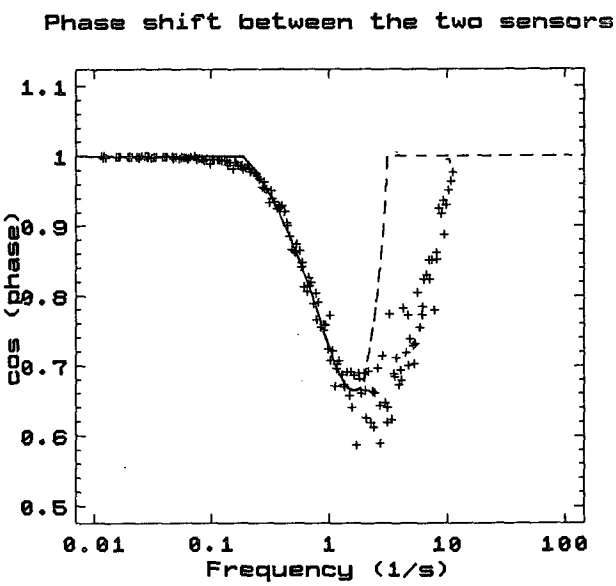

FIG. 5. Cosine of the phase shift between the relative humidity calculated from the calibrated Lyman-α and that calculated from the capacitive sensor, as a function of the frequency (s^{-1}, log coordinate). The solid and dashed lines are the correction applied to the capacitive signal.

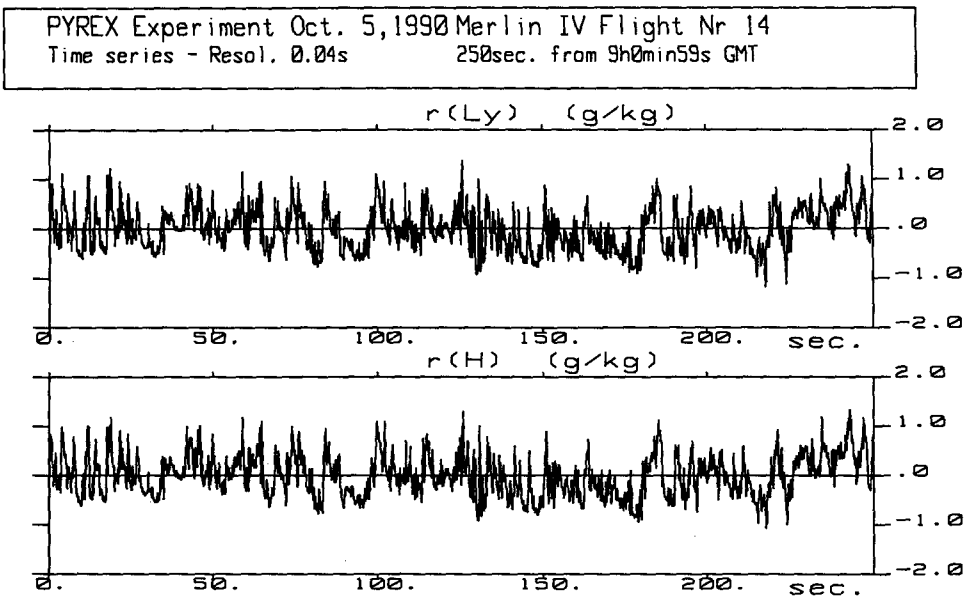

FIG. 6. Time series of the humidity mixing ratio (g kg^{-1}), calculated with the corrected capacitive sensor (bottom) and with the calibrated Lyman-α (top). Same sample as Fig. 1.

frequencies. For frequencies greater than about 3 s^{-1}, the energy is attenuated by more than an order of magnitude. At lower frequencies, both spectra are identical. This was encouraging enough to attempt to correct this attenuation in order to make this sensor able to measure turbulence. The process was the following:

1) Calculate the "true" turbulent relative humidity H_{Ly} from r_{Ly} and T with (2).

2) Calculate the attenuation of the spectral amplitude and the phase shift of relative humidity H deduced from the capacitive sensor [with (3)], and correct them. The amplitude and phase of H_{Ly} and H, as a function of frequency, were calculated with a fast Fourier transform (FFT). The amplitude and phase of H were then calibrated against those of H_{Ly}. The corrected signal H_c was then calculated with an inverse FFT from these corrected amplitude and phase.

3) Calculate the humidity mixing ratio with the corrected humidity H_C and the temperature with (2).

We propose here to apply a correction not only to the amplitude [e.g., as performed by Nicholls (1978) for the Rosemount temperature probe], but also to the phase of the signal, the latter being of importance for computation of the latent heat flux. Figure 4 shows the spectral energy ratio of the "true" humidity to the capacitive humidity, as well as the fit used to correct this ratio. Figure 5 presents the phase shift, with respect to the "true" signal, as well as the proposed correction. The set of data corresponds to four straight and level runs, each about 4–5 min. We see that the correction is important from the frequency of about 0.3 s^{-1}. The upper limit for energy correction is about 3 s^{-1}, because for higher frequencies the attenuation is too great (more than one order of magnitude). The upper limit for phase correction is about 2 s^{-1}, because for higher frequencies, phase behavior seems to be incoherent. Above these limits, the corrections are slowly reduced, as represented by the dashed-line sections on Figs. 4 and 5. This slow reduction of the correction avoids some numerical artifact on the signal, when calculating the time series as the inverse transform of the corrected spectral density and corrected phase.

4. Results with the corrected sensor

The corrected signal r_H is presented in Fig. 6 with the "true" signal r_{Ly}. The agreement between both signals is apparently very good. When compared to the noncorrected signal presented in Fig. 2, the improvement is obvious. This is confirmed in Fig. 7, which presents the energy spectrum of the corrected and uncorrected r_H, and of r_{Ly}. Up to 3 s^{-1}, the power spectrum of the corrected r_H is similar to that of r_{Ly}, and follows the turbulent $-2/3$ power law. The cospectrum and the phase spectrum of the latent heat flux, for the same sample, are presented in Figs. 8a and 8b, respectively. These figures clearly exhibit the underestimation of the cospectral energy and the phase shift between vertical velocity and moisture, in the frequency band ranging from 0.3 to 3 s^{-1}, when using the uncorrected capacitive sensor. On the contrary, with the corrected sensor, the cospectrum and the phase spectrum are similar to those calculated with the Lyman-α sensor throughout the whole frequency band contributing to the transfer.

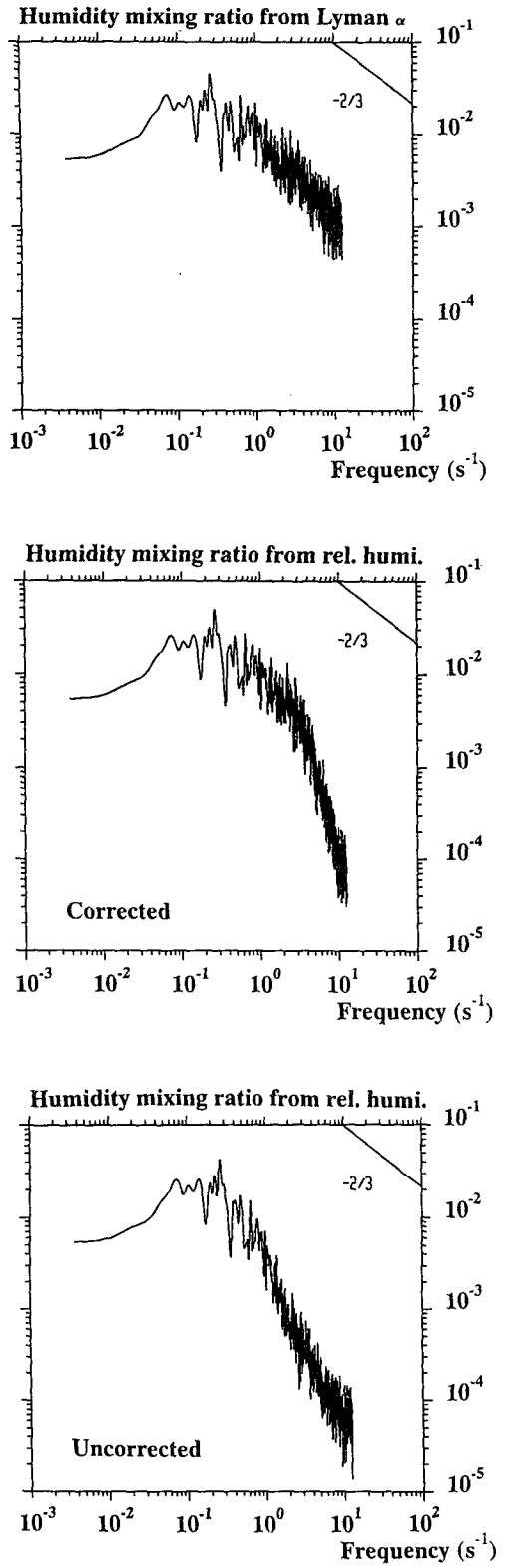

FIG. 7. Power spectrum of the humidity mixing ratio [$nS(n)$, (g^2 kg^{-2})], as a function of the frequency (s^{-1}); (bottom) uncorrected capacitive sensor, (middle) corrected capacitive sensor, (top) calibrated Lyman-α. Same sample as Fig. 1 and Fig. 3.

We can now use this calibrated sensor to determine the turbulent latent heat flux, and the variance of moisture. These quantities are presented in Figs. 9a and 9b in a comparison with the same quantities calculated with the "true" mixing ratio: we see that the use of the uncorrected capacitive sensor leads to a considerable underestimation of the flux as well as of the variance, whereas the computations with the corrected sensor are accurate. Low fluxes and variances correspond to measurements made over the land, during the transit toward the sea, whereas high values are linked to the marine ABL. We can note that the difference between the corrected and uncorrected fluxes is much more important over sea than over land. This has to be related to the characteristic scales of the transfer: over the sea, the measurements were performed at low altitude (40 m on average), whereas the legs over land were flown at about 300 m above the ground. According to Lenschow and Stankov (1986), the integral scale £ of a turbulent process, in the ABL, is scaled by the reduced altitude z/Z_i, where Z_i is the boundary layer thickness. Considering the flight altitude over the land and over the sea, the boundary layer thickness (600 m over land and 450 m over sea), and following the formulation proposed by Lenschow and Stankov, we found that $£_{wr} \approx 80$ m over land and $£_{wr} \approx 30$ m over sea, in other words that the characteristic scales contributing to the latent heat flux are much greater for the legs over the land than for the legs over the sea. The greater these scales, the less the constraints on the time response of the sensor. This explains why the time response of the uncorrected signal is quite sufficient over land. Another illustration of this difference in scales between the two areas is presented in Fig. 10: it represents the ratio of the frequency integral of the latent heat flux cospectrum, for the corrected and uncorrected signal, to the same integral calculated with the Lyman-α:

$$F_{wr}(n) = \frac{\int_{\ln(n_0)}^{\ln(n)} n\,\mathrm{Co}_{wr_H}(n)\,d[\ln(n)]}{\int_{\ln(n_0)}^{\ln(n)} n\,\mathrm{Co}_{wr_{Ly}}(n)\,d[\ln(n)]}, \qquad (5)$$

where n_0 is the lowest frequency of the sample. Two samples are represented in Fig. 10: the upper part of the figure deals with a low-altitude (35 m) leg over the sea, whereas the lower part deals with a 350-m altitude leg over land. For low frequencies (lower than 0.3 s^{-1}), the corrected and uncorrected integrals, calculated with the capacitive device, are similar to that calculated with the Lyman-α: the difference is lower than 10%. For frequencies greater than 0.2 s^{-1}, the two areas present different behavior: the sample at 350 m allows a precise computation with both corrected and uncorrected signals: the difference between the two is no greater than 5%. This can be explained by the fact that the frequencies greater than 0.3 s^{-1} (or, given the airspeed of

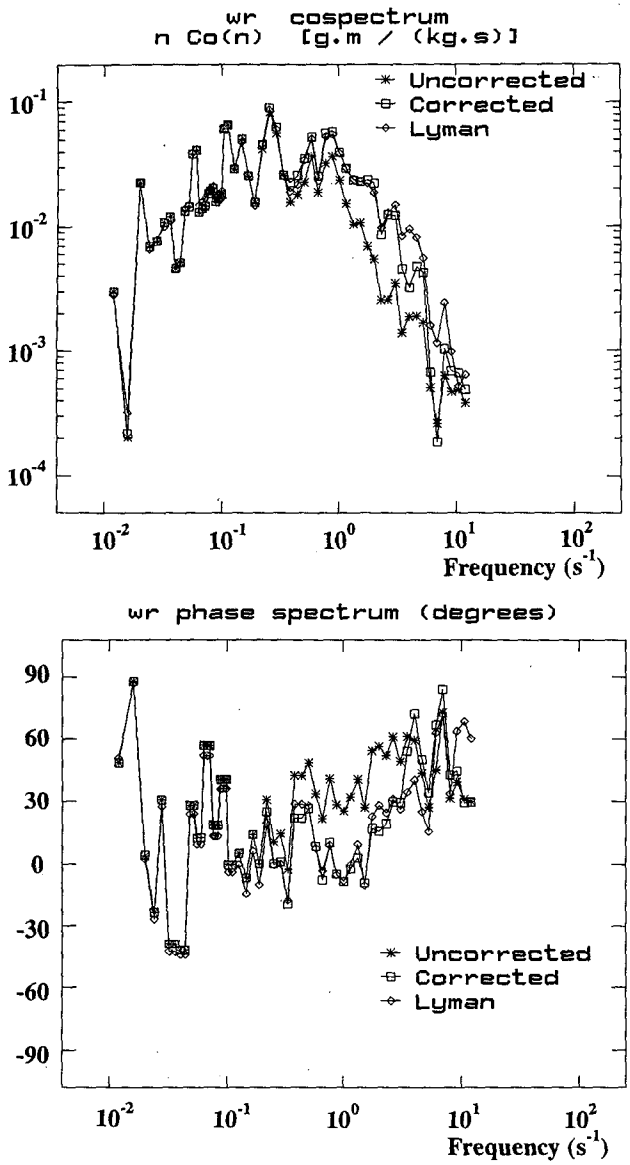

FIG. 8. (a) Latent heat flux cospectrum [$n\,Co(n)$, (g kg^{-1}) (m s^{-1})] calculated with the calibrated Lyman-α sensor (diamond), with the uncorrected (asterisk) and with the corrected (square) capacitive device. Same sample as Fig. 1 (35 m over the sea). (b) Phase spectrum of the latent heat flux, calculated with the calibrated Lyman-α sensor (diamond), with the uncorrected (asterisks) and with the corrected (square) capacitive device. Same sample as Fig. 9a.

the aircraft, the wavelengths lower than 300 m) do not contribute significantly to the transfer. At low altitude, on the contrary, the uncorrected flux is underestimated by more than 20%, and the contribution to the flux extends up to frequencies as high as 4 s^{-1} (or wavelengths greater than 25 m). This demonstrates that the capacitance sensor can be used for latent heat flux measurements without correction in convective boundary layers, provided that the altitude above ground level was high enough. For lower altitudes, the correction has to be made.

As already mentioned, calibration was applied, during the PYREX experiment, to two flights during which the Lyman-α device did not operate. These two flights (numbers 22 and 23) were performed on 4 and 5 November, respectively, over the same area (Mediterranean Sea) as for flight 14 (15 October), which was used for the calibration. To verify that the fluxes computed on flights 22 and 23 are correct, we can compare the bulk coefficient calculated from these fluxes to the

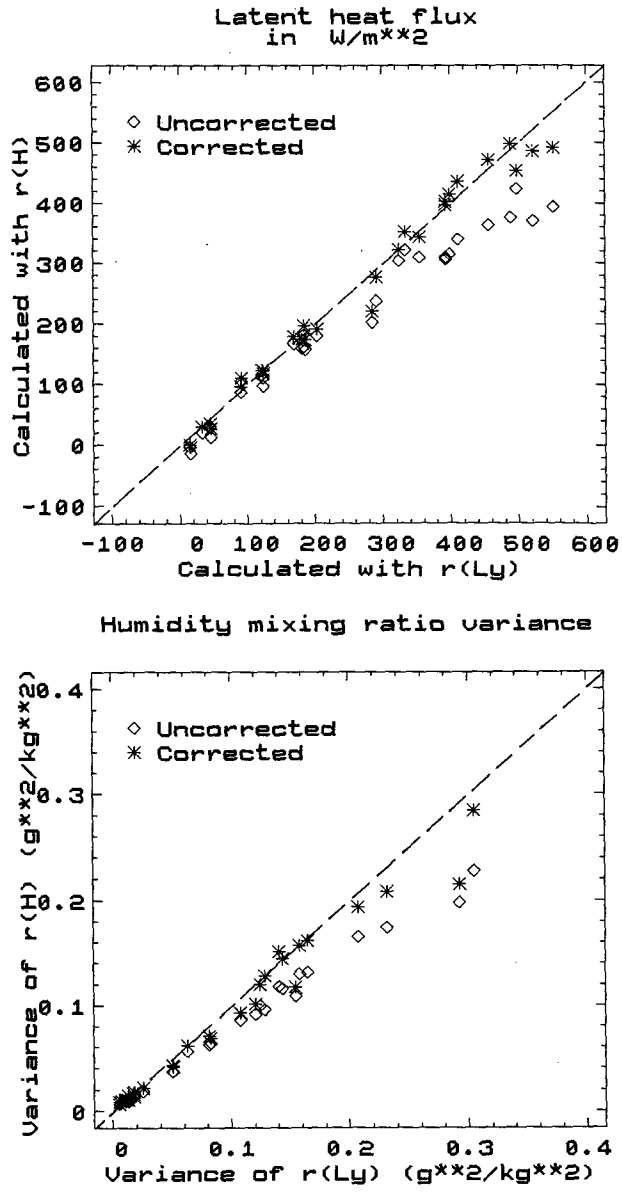

FIG. 9. (a) Latent heat flux (W m^{-2}) calculated with the calibrated Lyman-α vs that calculated with uncorrected (diamond) and corrected (asterisk) capacitive sensor. The dashed line is the 1:1 slope. (b) Same as (a) but for humidity mixing ratio variance (g^2 kg^{-2}).

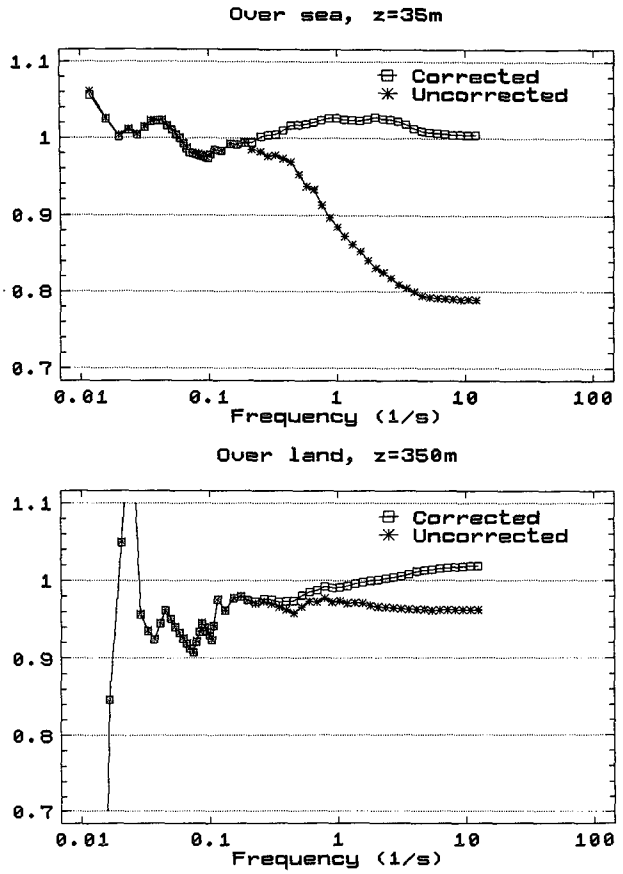

FIG. 10. Frequency vs the function $F_{wr}(n)$ [see Eq. (5) for definition] (top) for a leg flown at 40-m altitude above the sea; (bottom) for a leg performed at 350-m altitude above the land. The stars refer to the uncorrected moisture signal, whereas the squares refer to the corrected one.

same coefficient computed from the other flights of the experiment flown over the same area and during similar meteorological conditions, and for which the latent heat flux was calculated with the Lyman-α device. The bulk coefficient for latent heat C_E, also called Dalton number, is defined as follows:

$$C_E = \frac{\overline{w'r'_0}}{U_{10}(r_0 - r_{10})}, \qquad (6)$$

where the subscript 0 refers to the surface value, whereas the subscript 10 refers to the conventional altitude of 10 m. Here, U is the wind velocity. The calculation algorithm of U_{10}, r_0, and r_{10} from the aircraft data is developed in Hedde and Durand (1994). The latent heat flux, computed at an average altitude of 40 m, is considered to not significantly differ from its surface value. This hypothesis is also justified in Hedde and Durand (1994). The average value of C_E for flights 22 and 23 is 1.48 ± 0.23, whereas the other flights give a value of 1.34 ± 0.34. These two values are not significantly different, which validates the latent heat flux computation. This demonstrates that the calibration remains valid from one flight to another.

5. Conclusions

To summarize, the use of a capacitive humidity sensor appears to be possible as an alternative sensor for turbulence moisture measurement. This technique was successfully applied to two flights over the sea during the PYREX experiment, during which we had some problems with the Lyman-α sensor. The calibration of the device takes into account the amplitude attenuation, as well as the phase shift of the sensor, as a function of the frequency. This correction extends the time response from 0.2 up to 2 s^{-1}, which allows latent heat flux computation. The consequence of this correction on the latent heat flux value varies according to the characteristic length scales of the latent heat flux: it reaches about 20% at 40-m altitude over the sea, whereas it is no greater than 5% at higher altitudes (typically 300 m) over land, under convective conditions.

Numerous advantages can be found in using a capacitive device: it is less expensive than the Lyman-α sensor, and it does not necessitate an absolute calibration against, for example, a dewpoint hygrometer. So, when calibrated as explained in this paper, this sensor covers the whole frequency range, which contributes to the latent heat flux, and then can be used for turbulence measurements.

Acknowledgments. We want to express our gratitude to Philippe Bougeault, who managed the PYREX experiment, and to Michel André and his colleagues at the "Centre d'Aviation Météorologique," who operated Merlin IV during the experiment and provided us with the data used in this paper. This study was financially supported by the "Programme Atmosphère Météorologique et Océan Superficiel" of the "Institut National des Sciences de l'Univers."

REFERENCES

Abadie, G., 1984: Multi-sheet capacity hygrometers. *BNM Bull. French Met. Office,* **58,** 13–18.

——, G. Cocher, and C. Berne, 1991: Use of relative humidity sensors for plane measurement. *Proc. Seventh Symp. on Meteorological Observations and Instrumentation,* New Orleans, LA, Amer. Meteor. Soc., 247–249.

André, M., and M. P. LePipec, 1989: Technical presentation of the Merlin's radome: Calibration and data processing. *Proc. Int. Workshop of the Airborne Measurement of Wind, Turbulence and Position,* Oberpfaffenhofen, Germany, DLR Report 90-13, 42–46.

Bougeault, P., A. Jansa, J. L. Attié, I. Beau, B. Bénech, R. Benoit, P. Bessemoulin, J. Campins, B. Carissimo, J. L. Champeaux, M. Crochet, A. Druilhet, P. Durand, A. Elkhalfi, P. Flamant, A. Genoves, M. Georgelin, K. P. Hoinka, V. Klaus, E. Koffi, V. Kotroni, C. Mazaudier, J. Pelon, M. Petitdidier, Y. Pointin, D. Puech, E. Richard, T. Satomura, J. Stein, and D. Tannhauser, 1993: The atmospheric momentum budget over a major mountain range: First results of the PYREX field program. *Ann. Geophys.,* **11,** 395–418.

Brown, E. N., C. A. Friehe, and D. H. Lenschow, 1983: The use of pressure fluctuations on the nose of an aircraft for measuring air motion. *J. Climate Appl. Meteor.*, **22,** 171–180.

Buck, A. L., 1976: The variable-path Lyman-alpha hygrometer and its operating characteristics. *Bull. Amer. Meteor. Soc.*, **57,** 1113–1118.

C.A.M., 1989: General description of instrumented aircraft Merlin IV F-GMTO. *CAM Bull.*, **6.** [Available in CAM/CEV F-91220 Brétigny/Air.]

Druilhet, A., J. P. Frangi, D. Guedalia, and J. Fontan, 1983: Experimental studies of the turbulence structure parameters of the convective boundary layer. *J. Climate Appl. Meteor.*, **22,** 593–608.

Friehe, C. A., R. L. Grossman, and Y. Pann, 1986: Calibration of an airborne Lyman-alpha hygrometer and measurement of water vapor flux using a thermoelectric hygrometer. *J. Atmos. Oceanic Technol.*, **3,** 299–304.

Hedde, T., and P. Durand, 1994: Turbulence intensities and bulk coefficients in the surface layer above the sea. *Bound.-Layer Meteor.*, **71,** 415–432.

Lenschow, D. H., 1970: Airplane measurements of planetary boundary layer structure. *J. Appl. Meteor.*, **9,** 874–884.

——, and B. B. Stankov, 1986: Length scales in the convective boundary layer. *J. Atmos. Sci.*, **43,** 1198–1209.

Lind, R. J., and W. J. Shaw, 1991: The time-varying of an airborne Lyman-alpha hygrometer. *J. Atmos. Oceanic Tecnol.*, **8,** 186–190.

Nicholls, S., 1978: Measurements of turbulence by an instrumented aircraft in a convective atmospheric boundary layer over the sea. *Quart. J. Roy. Meteor. Soc.*, **104,** 653–676.

Weinheimer, A. J., and R. L. Schwiesow, 1992: A two-path, two-wavelength ultraviolet hygrometer. *J. Atmos. Oceanic Technol.*, **9,** 407–419.